

Rapidity-dependent spectra from a single-freeze-out model of relativistic heavy-ion collisions

Bartłomiej Biedroń*

AGH University of Science and Technology, Al. Mickiewicza 30, 30-059 Kraków, Poland

Wojciech Broniowski†

Institute of Physics, Świętokrzyska Academy, ul. Świętokrzyska 15, PL-25406 Kielce, Poland

The H. Niewodniczański Institute of Nuclear Physics, Polish Academy of Sciences, PL-31342 Kraków, Poland

(Received 20 October 2006; published 10 May 2007)

An extension of the single-freeze-out model with thermal and geometric parameters dependent on the spatial rapidity, α_{\parallel} , is used to describe the rapidity and transverse-momentum spectra of pions, kaons, protons, and antiprotons measured at the Relativistic Heavy Ion Collider at $\sqrt{s_{NN}} = 200$ GeV by the BRAHMS Collaboration. THERMINATOR is used to perform the necessary simulation, which includes all resonance decays. The result of the fit to the rapidity spectra in the range of the BRAHMS data is the expected growth of the baryon and strange chemical potentials with the magnitude of α_{\parallel} , whereas the freeze-out temperature is kept fixed. The value of the baryon chemical potential at $\alpha_{\parallel} \sim 3$, which is the relevant region for particles detected at the BRAHMS forward rapidity $y \sim 3$, is about 200 GeV, i.e., lies in the range of the values obtained for the highest SPS energy. The chosen geometry of the fireball has a decreasing transverse size as the magnitude of α_{\parallel} is increased, which also corresponds to decreasing transverse flow. This feature is verified by reproducing the transverse momentum spectra of pions and kaons at various rapidities. The strange chemical potential obtained from the fit to the K^+/K^- ratio is such that the local strangeness density in the fireball is compatible with zero. The resulting rapidity spectra of net protons are described qualitatively in the model. As a result of the study, the knowledge of the “topography” of the fireball is achieved, making other calculations possible. As an example, we give predictions for the rapidity spectra of hyperons.

DOI: 10.1103/PhysRevC.75.054905

PACS number(s): 25.75.Gz, 24.60.–k

I. INTRODUCTION

The study of particle abundances has been a major source of information concerning heavy-ion collisions. In fact, the agreement of the particle ratios with simple predictions of statistical models is a key argument for thermalization of the formed system [1–4]. Up to now the numerous studies of the particle ratios [5–23] were falling into two basic categories: the so-called 4π studies at low energies (SIS, AGS) and the studies at midrapidity for approximately boost-invariant systems at highest energies (Relativistic Heavy Ion Collider (RHIC)). The 4π studies involve three-momentum integrals of the statistical distribution functions, with the multiplicity of species i given by $N_i = V \int d^3 p f_i(\sqrt{m_i^2 + p^2})$, thus providing information on volume-averaged thermal parameters of the system in a very simple way. The inclusion of resonance decays [24–26], crucial for the success of the approach, is also straightforward, because the detection of the products with full angular coverage is insensitive to the decay kinematics or flow effects; once the resonance has decayed, its products are registered. The other simple situation arises when the system is nearly boost invariant. To a sufficiently good accuracy this is the case at midrapidity for the RHIC energies, where the particle yields dN/dy change only by a few percentages in the rapidity window $|y| < 1$. The assumption of the boost invariance of the fireball leads again to very simple formulas.

Although the particles detected at midrapidity are collected from various parts of the fireball, not only from the very central region, their ratios are the same as in the 4π calculation. This is because for $dN_i/dy = \int d^2 p_{\perp} d^3 N_i / (d^2 p_{\perp} dy)$ we have from the boost invariance [27]

$$\frac{dN_i/dy}{dN_j/dy} = \frac{\int dy dN_i/dy}{\int dy dN_j/dy} = \frac{N_i}{N_j}. \quad (1)$$

This obvious general formula finds an explicit manifestation in specific boost-invariant models. The result also holds when resonance decays are included; see Ref. [28] for a derivation in the framework of the Cooper-Frye [29] formalism.

When the system is not boost invariant [30,31] the above simplifications no longer hold. The situation is illustrated in Fig. 1. Particles detected at a given pseudorapidity η (parallel lines in the figure) originate from different pieces of the fireball (gray blobs). Thermal conditions (temperature, chemical potentials, flow) change from piece to piece, which must be properly included. In addition, the effects of the longitudinal flow (indicated by arrows) must be incorporated, and the kinematics of resonance decays (dashed lines) becomes relevant. Although the resulting formalism for particle spectra remains conceptually simple and is based on the standard Cooper-Frye treatment, the calculation is no longer semianalytic and a full-fledged simulation is necessary to accomplish the goal.

In the analysis of this article we use THERMINATOR—the THERMal heavy IoN generATOR [32]—to generate the Monte Carlo events in a suitably modified single-freeze-out

*Electronic address: rockhouse@dione.ifj.edu.pl

†Electronic address: Wojciech.Broniowski@ifj.edu.pl

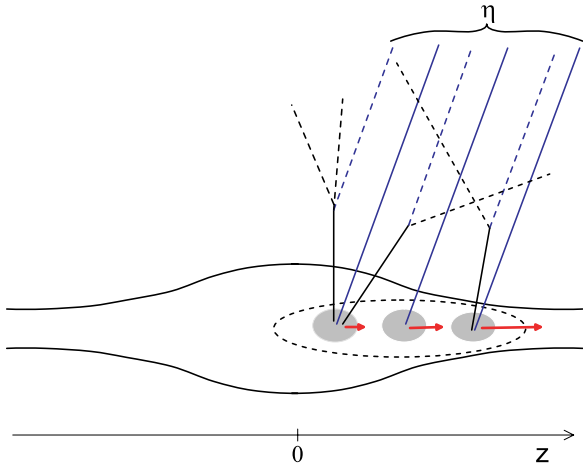


FIG. 1. (Color online) Emission of particles from a boost-noninvariant fireball. The horizontal (vertical) axis indicates longitudinal coordinate z (transverse coordinate ρ). Particles emitted with the same value of pseudorapidity η originate from different regions of the fireball indicated by the gray blobs (they also are emitted at different times). The thermal conditions and flow (indicated by arrows) in these regions are different. The solid lines indicate tracks of primordial particles, whereas the dashed lines show products of resonance decays. The dashed ellipse indicates the relevant region for a given η , which spans about two units of the spatial rapidity α_{\parallel} .

model of Ref. [27]. The extension to the boost-noninvariant case consists of two basic elements. The first one (geometric) is the choice of the shape of the freeze-out hypersurface Σ and collective expansion. The other one incorporates the dependence of the thermal parameters on the position within the hypersurface Σ . Specifically, in our treatment the transverse size and the chemical potentials depend on the spatial rapidity $\alpha_{\parallel} = \text{arctanh}(z/t)$, where z and t are the longitudinal and time coordinates on the freeze-out hypersurface. Although the boost-noninvariant model has quite a few parameters, as listed at the end of Sec. II, they can be fitted independently to various combinations of the data, leaving little freedom. For instance, the α_{\parallel} dependence of the baryon and strange chemical potentials is fixed with the ratios of protons to antiprotons and K^+ to K^- . The result in the range of the BRAHMS data is the expected growth of the baryon and strange chemical potentials with $|\alpha_{\parallel}|$. The value of the baryon chemical potential μ_B at $\alpha_{\parallel} \sim 3$, which is the relevant region for particles detected at the BRAHMS forward rapidity, $y \sim 3$, is about 200 GeV. This value is in the range of the values of the thermal fits for the highest SPS energy, thus we confirm the recent findings by Roehrich [33] that the thermal conditions at RHIC at forward rapidities, $y \sim 3$, correspond to the SPS conditions at midrapidity. Details of our procedure of determining the dependence of thermal parameters on α_{\parallel} are explained in Sec. III. Our strategy, as usual, is to fix the features of the fireball with the well-measured spectra of particles: pions, kaons, protons, and antiprotons. The strange chemical potential obtained from the fit to the K^+/K^- ratio is such that the local strangeness density on the freeze-out hypersurface Σ is compatible with zero. The experimental [34] rapidity spectra of net protons, $p - \bar{p}$, are reproduced

qualitatively in the model, displaying the correct shape but overshooting the data at larger rapidities by about 50%. The chosen geometry of the fireball incorporates a decreasing transverse size as $|\alpha_{\parallel}|$ is increased, which simultaneously results in a decreasing transverse flow. This choice is verified in Sec. III by reproducing the spectra $d^2N/(2\pi p_T dp_T dy)$ at a fixed y of pions and kaons at $\sqrt{s_{NN}} = 200$ GeV from the BRAHMS Collaboration [35]. These transverse-momentum spectra exhibit slopes that become steeper with rapidity.

As a result of our study, we obtain the “topography” of the fireball, which can be the ground for other more detailed studies, discussed under Conclusion.

II. THE SINGLE FREEZE-OUT MODEL

The single-freeze-out model is described in detail in Refs. [27,28,36]. Here we review the main assumptions and the formalism of describing the expansion and particle decays.

- (i) At a certain stage of evolution of the fireball the thermal equilibrium between hadrons is reached. Most probably, hadrons are “born” already in such an equilibrated state. The local particle phase-space densities have the form of the Fermi-Dirac or Bose-Einstein statistical distributions. The particles generated at freeze-out are termed *primordial*. For simplicity of the model we do not include the γ nonequilibrium factors of Ref. [37] used in several recent analyses [18,20,21].
- (ii) The thermodynamic parameters are the freeze-out temperature T and three chemical potentials: baryon, μ_B , strange, μ_S , and μ_{I_3} , related to the third component of isospin. In a boost-noninvariant model the values of these parameters depend on the position within the freeze-out hypersurface Σ .
- (iii) In the boost-noninvariant model the shape of the fireball is nontrivial in the longitudinal direction. In this article we retain the azimuthal symmetry.
- (iv) The velocity field of the collective expansion is chosen in the form of the Hubble flow [38], providing the longitudinal and transverse flow to the system. Again, in the boost-noninvariant model the functional form of the velocity field may depend on the longitudinal position.
- (v) The evolution after freeze-out consists solely of free streaming and the *decays of resonances*, which may proceed in cascades. All resonances from the Particle Data Tables [39] are incorporated.
- (vi) Elastic rescattering among particles after the chemical freeze-out is ignored and the model may be viewed as an approximation to a more detailed evolution, taking into account different time scales for various hadronic processes [40–45].

The single freeze-out concept complies to the *explosive scenario* at RHIC [14]. Moreover, the approach reproduces very efficiently the particle abundances, the transverse-momentum spectra, including particles with strangeness [36], produces very reasonable results for the resonance production [46], the charge balance HBT functions in rapidity [47], the elliptic flow [48], the HBT radii [49], and the transverse energy

[50–52]. Recently, with the help of RQMD [53], Nonaka and Bass have found (cf. Figs. 16 and 17 of Ref. [54]) that the elastic rescattering effects are not very significant for the midrapidity p_T spectra of pions and kaons, where the changes are at the level of 10–20% (contrary, according to Ref. [54] hadronic rescattering is important for protons and multistrange baryons). One can argue in favor of the single-freeze-out scenario as follows: resonance decays “cool” the spectra [27]. As the result, the original ~ 165 -MeV spectra from the chemical freeze-out look, after feeding from resonances, approximately as ~ 130 -MeV spectra, which would be obtained at the lower temperature of the thermal freeze-out. Thus elastic rescattering becomes innocuous. Certainly, more studies are desirable here, in particular an “afterburner” performing elastic rescattering could be run on top of our simulation. It would help to achieve a more accurate collision picture, with the elastic rescattering processes taken fully into account.

Popular choices of the freeze-out hypersurface and the collective velocity field are discussed in detail in Ref. [55]. In this work we modify in a very simple way the original boost-invariant single-freeze-out model of Ref. [27,28,36] by making the transverse size of the fireball dependent on the spatial rapidity. We use the freeze-out hypersurface parametrized as

$$x^\mu = \begin{pmatrix} t \\ x \\ y \\ z \end{pmatrix} = \begin{pmatrix} \tau \cosh \alpha_\perp \cosh \alpha_\parallel \\ \tau \sinh \alpha_\perp \cos \phi \\ \tau \sinh \alpha_\perp \sin \phi \\ \tau \cosh \alpha_\perp \sinh \alpha_\parallel \end{pmatrix}. \quad (2)$$

The parameter α_\parallel is the *spatial rapidity*, whereas α_\perp is related to the transverse radius as

$$\rho = \sqrt{x^2 + y^2} = \tau \sinh \alpha_\perp. \quad (3)$$

The four-velocity field is chosen to follow the Hubble law

$$u^\mu = x^\mu / \tau. \quad (4)$$

We note that the longitudinal flow is $v_z = \tanh \alpha_\parallel = z/t$ (as in the one-dimensional Bjorken model [56]), whereas the transverse flow (at $z = 0$) has the form $v_\rho = \tanh \alpha_\perp$.

The new element of the parametrization of this article, which implements the departure from boost invariance, is the selection of boundaries for the fireball. In the boost invariant model ρ was limited by the space-independent parameter ρ_{\max} , or $0 \leq \alpha_\perp \leq \alpha_\perp^{\max}$. Now we take

$$0 \leq \alpha_\perp \leq \alpha_\perp^{\max}(\alpha_\parallel) \equiv \alpha_\perp^{\max}(0) \exp\left(-\frac{\alpha_\parallel^2}{2\Delta^2}\right). \quad (5)$$

The interpretation of this formula is clear: as we depart from the center by increasing $|\alpha_\parallel|$, we simultaneously reduce α_\perp , or ρ_{\max} . The rate of this reduction is controlled by a new model parameter, Δ . Because in our model the flow is linked to the position via Eq. (4), we also have less transverse flow as we increase $|\alpha_\parallel|$. This feature will show in the p_T spectra presented in Sec. III. We may also use more conveniently the parameter

$$\rho_{\max}^{(0)} = \sinh \alpha_\perp^{\max}(0). \quad (6)$$

Thus the geometry and expansion of the fireball is described by three parameters: τ , $\rho_{\max}^{(0)}$, and Δ .

With the standard parametrization of the particle four-momentum in terms of rapidity y and the transverse mass m_\perp ,

$$p^\mu = (m_\perp \cosh y, p_\perp \cos \varphi, p_\perp \sin \varphi, m_\perp \sinh y), \quad (7)$$

we find with Eqs. (2) and (4)

$$p \cdot u = m_\perp \cosh(\alpha_\perp) \cosh(\alpha_\parallel - y) - p_\perp \sinh(\alpha_\perp) \cos(\phi - \varphi), \quad (8)$$

and

$$\begin{aligned} d^3 \Sigma \cdot p &= d\alpha_\parallel d\phi \rho d\rho \times [m_\perp \sqrt{\tau^2 + \rho^2} \cosh(\alpha_\parallel - y) \\ &\quad - p_\perp \rho \cos(\phi - \varphi)] \\ &= \tau^3 d\alpha_\parallel d\phi \sinh \alpha_\perp d\alpha_\perp p \cdot u, \end{aligned} \quad (9)$$

where $d^3 \Sigma^\mu$ is the volume element of the hypersurface. With the assumed azimuthal symmetry the Cooper-Frye [29] formalism then yields the following expression for the momentum density of a given species of primordial particles:

$$\begin{aligned} \frac{d^2 N}{2\pi p_T dp_T dy} &= \tau^3 \int_{-\infty}^{\infty} d\alpha_\parallel \int_0^{\alpha_\perp^{\max}(\alpha_\parallel)} d\alpha_\perp \int_0^{2\pi} d\phi \\ &\quad \times p \cdot u f(\beta p \cdot u - \beta \mu(\alpha_\parallel)), \quad (10) \\ f(z) &= \frac{1}{(2\pi)^3} \frac{1}{\exp z \pm 1}, \end{aligned}$$

where $p \cdot u$ from Eq. (8) is taken at $\varphi = 0$, $f(z)$ is the statistical distribution function (with + for fermions and – for bosons), $\beta = 1/T$, and

$$\mu(\alpha_\parallel) = B\mu_B(\alpha_\parallel) + S\mu_S(\alpha_\parallel) + I_3\mu_{I_3}(\alpha_\parallel), \quad (11)$$

with B , S , and I_3 denoting the baryon number, strangeness, and the third component of isospin of the particle. Thus we admit the dependence of chemical potentials on the spatial rapidity. This is of course necessary if we wish to describe in the framework of a statistical model the increasing density of net protons as we move from midrapidity toward the fragmentation region.

The temperature T also in general depends on α_\parallel . The best model-building strategy here would be to use the universal Cleymans-Redlich chemical freeze-out curve [12] in the μ_B - T space (for a recent status see Ref. [18,57]). That way the functional dependence of μ_B on α_\parallel induces unambiguously the dependence of T on α_\parallel . In this work, however, we apply the model for not too large values of the rapidity, $|y| \leq 3.3$, and it will turn out that the obtained values for μ_B are less than ~ 250 MeV. From $\mu_B = 0$ to $\mu_B = 250$ MeV the universal freeze-out curve gives a practically constant value of T . For instance, at SPS ($Pb + Pb$, $\sqrt{s_{NN}} = 17$ GeV) one has [16] $T = 164$ MeV, $\mu_B = 229$ MeV, $\mu_S = 54$ MeV, and $\mu_{I_3} = -7$ MeV, with the value of T equal within errors to the RHIC value of 165 MeV. For this reason in the present analysis we fix the freeze-out temperature at a constant (independent of the spatial rapidity) value,

$$T = 165 \text{ MeV}. \quad (12)$$

If modeling were made for larger values of the rapidity and/or lower collision energies, the dependence of T on α_\parallel should be incorporated according to the prescription based on the

universal freeze-out curve. Eventually, we expect that when the fragmentation region is approached, T becomes very small and μ_B reaches the value of the order of 1 GeV.

Another qualitative argument for the approximate constancy of T at moderate values of $|\alpha_{\parallel}|$ may be inferred directly from the BRAHMS data. From the measured rapidity spectra (cf. Fig. 5), obviously, the yields of pions and kaons decrease with y . Thus, one needs to decrease the size of the emitting source, decrease the freeze-out temperature, or both. The decrease of temperature affects more strongly the particles with larger masses, because the thermal factor is approximately $\exp(-\sqrt{m^2 + \vec{p}^2}/T)$. Therefore, if we introduced variation of the temperature with the spatial rapidity, it would result in a faster drop with y of the pion yields compared to the kaons. Certainly the data excludes this situation, because the ratio of dN_{π}/dy to dN_K/dy is, within a few percentages, independent of y in the BRAHMS rapidity coverage. Therefore we must keep T constant (within a few percentages), and the remaining possibility is the decrease of the source size with $|\alpha_{\parallel}|$. Resonance decays complicate the above qualitative argument, but with the help of a numerical simulation we confirm it. Another way of providing the drop of yields with rapidity is to incorporate the γ nonequilibrium factors [37] dependent on α_{\parallel} , which may dilute the system as $|\alpha_{\parallel}|$ increases. We do not explore this possibility here.

For convenience, we parametrize functionally the dependence of the chemical potentials at low values of $|\alpha_{\parallel}|$ as follows:

$$\mu_i(\alpha_{\parallel}) = \mu_i(0)[1 + A_i\alpha_{\parallel}^{2.4}], \quad i = B, S, I_3. \quad (13)$$

The chosen power of 2.4 works somewhat better than 2. Of course, any convenient and sufficiently rich parametric form is admissible here, as it is fitted to the data (see Sec. III) and the introduced parameters effectively are not free. By ‘‘low’’ $|\alpha_{\parallel}|$ we mean the values relevant to the BRAHMS data, covering $|y| \leq 3.3$.

Formula (10) provides the spectra of the primordial particles. The following evolution of the system consists of free streaming, with resonances decaying into the daughter particles. We use THERMINATOR to perform the simulation. The code incorporates all the **** and *** resonances. Following the scheme of SHARE [58] it excludes all * resonances, and practically all ** resonances listed in the Particle Data Tables [39]. Each resonance decays at the time controlled by its lifetime, $1/\Gamma$. In the resonance’s rest frame the decay at time t occurs with the probability density $\Gamma \exp(-\Gamma t)$. The two-body or three-body decay channels are incorporated and the values of the branching ratios are taken from the Particle Data Tables. Heavy resonances may of course decay in cascades.

Let us summarize the model parameters. We have the universal freeze-out-temperature T , three chemical potentials at midrapidity, $\mu_B(0)$, $\mu_S(0)$, $\mu_{I_3}(0)$, three parameters A_B , A_S , and A_{I_3} of Eq. (13) describing the dependence of the chemical potentials on the spatial rapidity, and three geometry/expansion parameters: the proper time τ , the transverse size at midrapidity, $\rho_{\max}^{(0)}$, and the parameter Δ controlling the spatial rapidity dependence of the transverse size. Except for T taken to have the value (12) obtained in earlier thermal

analyses of particle ratios [27], the remaining parameters are fitted to the BRAHMS data [34,35] for the double differential spectra $d^2N/(2\pi p_T dp_T dy)$.

III. RESULTS

We first describe our fitting strategy, which with many parameters present must be done with care. We wish to have a good starting point for the parameters describing the chemical potentials. Practice shows that to a very good approximation the statistical distributions are very well approximated by the Boltzmann factors. Then the integrand of Eq. (10) contains the factor $\exp[-\beta m_{\perp} \cosh(\alpha_{\perp}) \sinh(\alpha_{\parallel} - y) + \beta \mu(\alpha_{\parallel})]$. Because of this the relevant integration range in α_{\parallel} is sharply peaked around $\alpha_{\parallel} \simeq y$ (the half-width is about one unit of α_{\parallel}) and the chemical potentials entering the formula are taken approximately at $\mu_i(\alpha_{\parallel}) \simeq \mu_i(y)$. Thus the factors $\exp[\beta \mu(y)]$ can be taken in front of the integration. If it were not for the resonance decays which modify the result (and are included in the full simulation) we would have to a good approximation the following relations:

$$\begin{aligned} \frac{p}{\bar{p}} &\simeq \exp(2\beta\mu_B), \\ \frac{K^+}{K^-} &\simeq \exp(2\beta\mu_S), \quad (\text{approximate formulas}) \quad (14) \\ \frac{\pi^+}{\pi^-} &\simeq \exp(2\beta\mu_{I_3}). \end{aligned}$$

The symbols on the left-hand side denote the ratios of yields of the specified particles at a fixed y and integrated over p_T . These are known from the data, thus we can invert

$$\mu_B(y) = \frac{1}{2}T \log(p/\bar{p}), \quad (\text{approximate formula}) \quad (15)$$

and so on. With the help of this form we set the starting values of the parameters $\mu_i(0)$ and A_i , which are then iterated. The iteration proceeds as follows: for a given set of parameters we run the full THERMINATOR simulation, which generates events. We first optimize the baryon-number parameters $\mu_B(0)$ and A_B with the help of the ratio of the p and \bar{p} rapidity spectra, then the strangeness parameters $\mu_S(0)$ and A_S using the K^+ to K^- ratio, then we go back again to the baryon parameters, etc., and loop until a fixed is reached. The isospin parameters $\mu_{I_3}(0)$ and A_{I_3} are consistent with zero and thus irrelevant. The Δ parameter is fixed with the pion rapidity spectra $dN_{\pi^{\pm}}/dy$. The optimum value is

$$\Delta = 3.33. \quad (16)$$

The result of our optimization for the chemical potentials is shown in Fig. 2. The optimum parameters are

$$\begin{aligned} \mu_B(0) &= 19 \text{ MeV}, \quad \mu_S(0) = 4.8 \text{ MeV}, \\ \mu_{I_3}(0) &= -1 \text{ MeV}, \quad A_B = 0.65, A_S = 0.70, A_{I_3} = 0. \end{aligned} \quad (17)$$

We observe the expected behavior for the baryon chemical potential, which increases with $|\alpha_{\parallel}|$. The value at the origin is 19 MeV, somewhat lower than the earlier midrapidity fits made in boost-invariant models in Refs. [15,27], yielding 26 MeV.

The lower value in our case is well understood. The previous midrapidity fits include the data in the range $|y| \leq 1$. This range collects the particles emitted from the fireball at $|\alpha_{\parallel}| \leq 2$, hence the value of μ_B in the previous midrapidity fits is an average of our $\mu_B(\alpha_{\parallel})$ over the range, approximately, $|\alpha_{\parallel}| \leq 2$, with some weight proportional to the particle abundance. This qualitatively explains the effect of a lower value of our $\mu_B(0)$ than in the boost-invariant models. A similar effect occurs for μ_S . We do not incorporate corrections for the feed-down from weak decays (em i.e., all decays are included), because this is the policy of Ref. [34] for the treatment of p and \bar{p} .

We note that at $\alpha_{\parallel} = 3$ the value of μ_B is 200 MeV, more than 10 times larger than at the origin. This value is comparable to the highest-energy SPS fit ($\sqrt{s_{NN}} = 17$ GeV), where $\mu_B \simeq 230$ MeV. The behavior of the strange chemical potential is qualitatively similar. It also increases with $|\alpha_{\parallel}|$, growing from 5 MeV at the origin to 50 MeV at $\alpha_{\parallel} = 3$. The ratio $\mu_B(\alpha_{\parallel})/\mu_S(\alpha_{\parallel})$ is very close to a constant, $\simeq 4$ – 3.5 , as can be seen in the bottom panel of Fig. 2.

The points in the top panel of Fig. 2 show the result of the naive calculation of Eqs. (14) and (15). We note that these points are very close (in particular for the strangeness case)

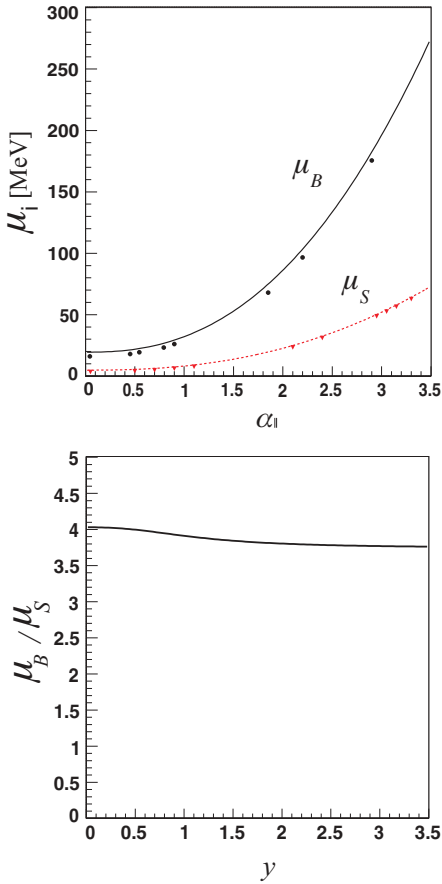


FIG. 2. (Color online) (Top) The model baryon and strange chemical potentials plotted as functions of the spatial rapidity. Parameters of Eq. (13) are obtained from the fit to the BRAHMS data [34,35]. The points represent a naive calculation based of Eq. (15). (Bottom) The ratio of the baryon to strange chemical potentials, μ_B/μ_S .

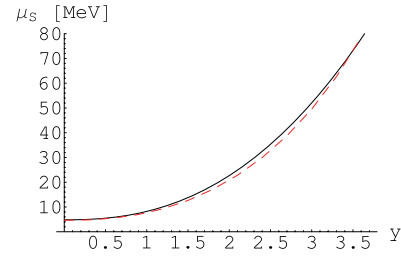


FIG. 3. (Color online) Comparison of the strange chemical potential obtained from the fit to the data (solid line) and from the condition of zero local strangeness density, $\rho_S = 0$ (dashed line).

to the result of the full-fledged fit of our model. This is of practical significance, because the application of Eqs. (14) and (15) involves no effort, whereas the model calculation incorporating resonance decays, flow, etc., is costly.

There is another important point. In thermal models one may obtain the local value of the strange chemical potential, μ_S , at a given μ_B with the condition of the vanishing strangeness density, $\rho_S = 0$. The result is shown in Fig. 3, where we compare the strange chemical potential obtained from the fit to the data (solid line) and from the condition of zero local strangeness density at a given $\mu_B(\alpha_{\parallel})$. The two curves turn out to be virtually the same. This shows that the net strangeness density in our fireball is, within uncertainties of parameters, *compatible with 0*. This is not obvious from the outset, as the condition of zero strangeness density is not assumed in our fitting procedure. Although this feature is natural in particle production mechanisms, in principle only the total strangeness, integrated over the whole fireball, must be initially zero. Variation of the strangeness density with α_{\parallel} is admissible, but turns out not to occur.

Figure 4 shows the quality of our fit for the parameters of chemical potentials, Eq. (17). We show the measured ratios of p/\bar{p} , K^+/K^- , and π^+/π^- as a function of rapidity y [34,35] and the results of fit made with help of the simulation with THERMINATOR. We note a very reasonable agreement. The error bars on the model points are statistical errors due to the finite size of the sample (we use 2500 simulated events in this plot). The flat character of the π^+/π^- ratio indicates that the value of the isospin chemical potential is consistent with zero at all spatial rapidity values.

In Fig. 5 we show the comparison of obtained rapidity spectra of π^+ , K^+ , and K^- to the experimental data. The experimental yields for the pions are corrected for the feed-down from the weak decays as described in Ref. [35]. For that reason for the case of π^+ we give the model predictions with the full feeding from the weak decays (solid line) and with no feeding from the weak decays at all (dashed line). We note a quite good quantitative agreement, with the data falling between the two extreme cases. We recall that the behavior on rapidity of dN/dy is controlled by the Δ parameter of Eq. (5). The spectra of π^- are not shown, since they are practically equal to the case of π^+ . The spectra of K^+ and K^- are also quite well reproduced.

Figure 6 displays the rapidity spectra of protons and antiprotons, as well as their difference $p - \bar{p}$, i.e. the *net* protons. Because the p and \bar{p} data carry no feed-down

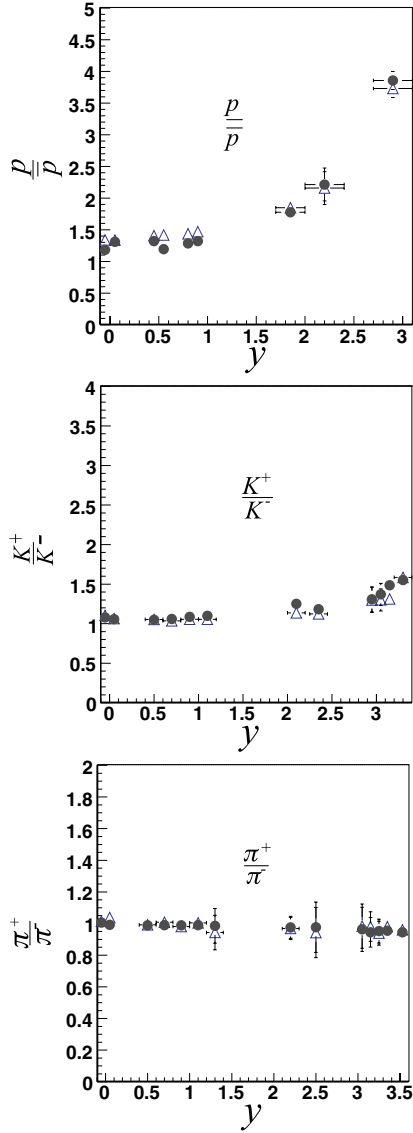


FIG. 4. (Color online) Dependence of particle ratios on rapidity: (top) – p/\bar{p} ; (middle) – K^+/K^- ; (bottom) – π^+/π^- . The open triangles are the Brahm's data [34,35], whereas the filled circles show the result of the model simulation with THERMINATOR. The model parameters are given in Eq. (17). The data for p and \bar{p} are not corrected for the feed-down from weak decays [34].

corrections for weak decays [34], one should compare the solid lines to the data. The shape of the p and \bar{p} spectra is properly reproduced, but the model overshoots the data by about 50%. This feature occurs at all rapidities, also at midrapidity. The mismatch could be improved by decreasing T by a few percentages and redoing the whole analysis, but we do not take the effort here, holding to the value (12) obtained from global fits to all RHIC data for the particle yields at midrapidity. We provide, however, the results of the model calculation with no feeding from the hyperon decays, since it provides some measure of the systematic uncertainties in determining the proton and antiproton yields.

We see from the bottom panel of Fig. 6 that the qualitative growing of the net-proton spectrum with y is obtained. Note

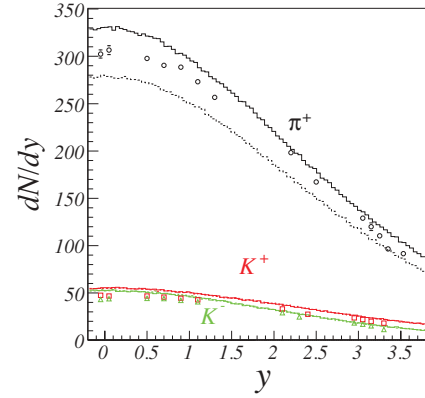


FIG. 5. (Color online) Rapidity spectra of π^+ , K^+ , and K^- . The data points come from the BRAHMS Collaboration [34,35] (circles- π^+ , squares- K^+ , triangles- K^-), whereas the histogram lines show the result of the model simulation with THERMINATOR. For π^+ the solid (dashed) line corresponds to the full feeding (no feeding) from the weak hyperon decays. The model parameters are from Eq. (17). The experimental pion yields are corrected for weak decays as described in Ref. [35].

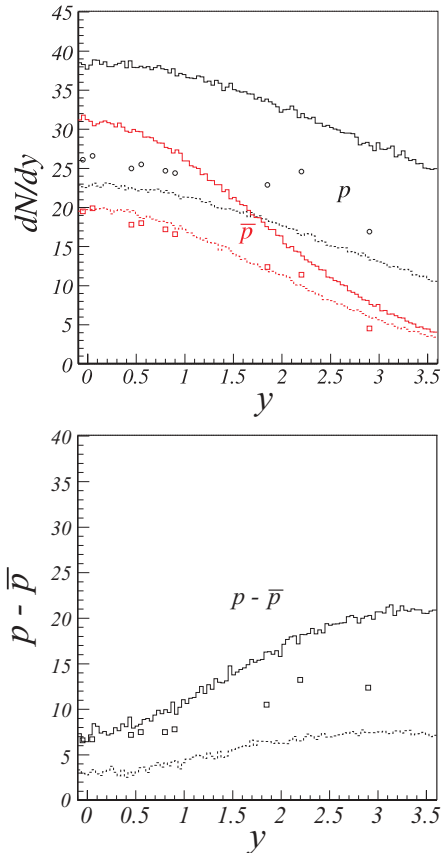


FIG. 6. (Color online) (Top) The rapidity spectra of p and \bar{p} . (Bottom) Spectrum of net protons, $p - \bar{p}$. The data points come from the BRAHMS Collaboration [34,35], whereas the solid (dashed) histogram lines show the result of the model simulation with THERMINATOR with full feeding (no feeding) from the weak hyperon decays. Data points should be compared to the model with full feeding (solid lines). The model parameters are from Eq. (17).

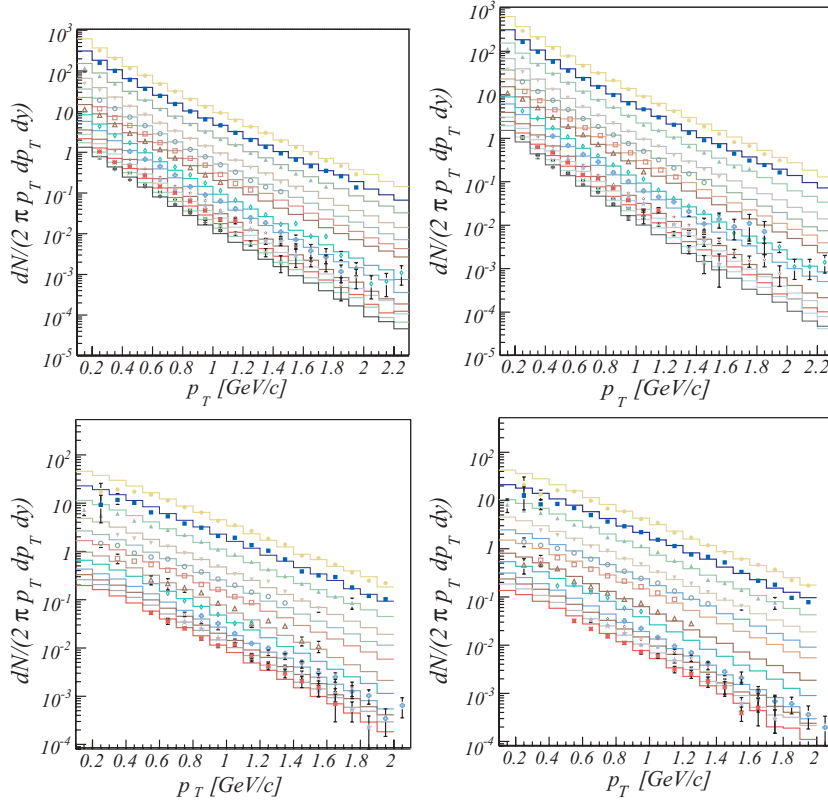


FIG. 7. (Color online) The p_T spectra of π^+ (top left), π^- (top right), K^+ (bottom left), and K^- (bottom right) in the subsequent BRAHMS rapidity bins, see the text for details. The data points come from Ref. [35], whereas the histogram lines show the result of the model simulation with THERMINATOR.

that predictive power is left for this observable, as only the ratio \bar{p}/p is used to fit μ_B at each value of y . Another combination, such as, e.g., $p - \bar{p}$, is left as a prediction. The growth has a simple explanation on the ground of our statistical

model, because approximately $p - \bar{p} \sim \sinh(\mu_B(y)/T)$ times the y -dependent source function, see Eq. (10). The observed increase with y is driven by the growth of $\mu_B(y)$ which overcomes the decrease caused by the reduced size of the

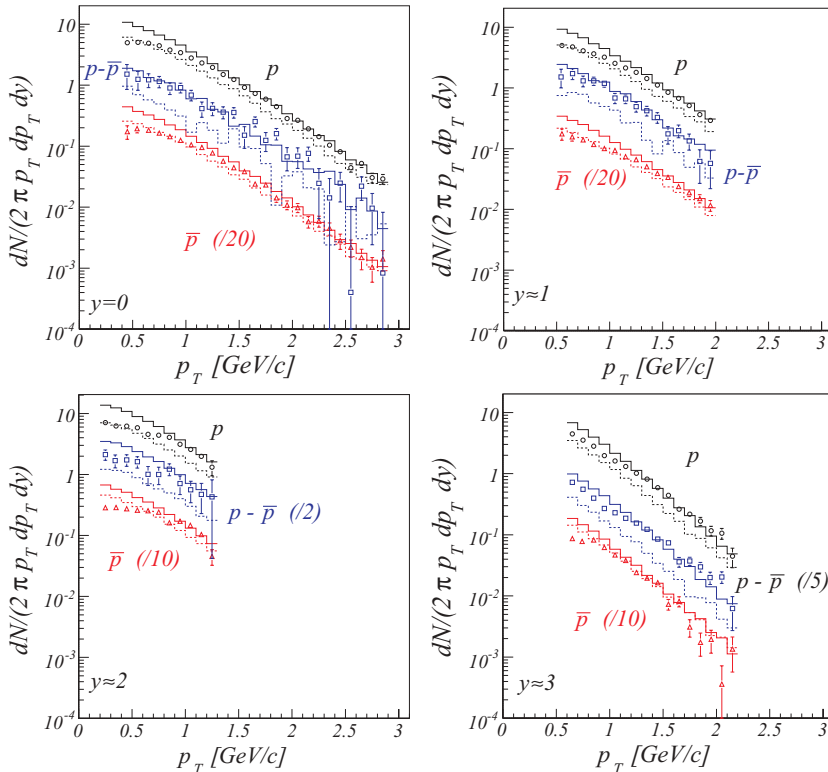


FIG. 8. (Color online) The proton, antiproton, and net-proton transverse momentum spectra at $y \simeq 0, 1, 2, 3$. The antiproton spectra and the net-proton spectra at $y \simeq 3$ have been divided by 10. The data points come from the BRAHMS Collaboration [34] and contain no weak-decay corrections. Solid (dashed) histogram lines show the result of the model simulation with full feeding (no feeding) from the weak hyperon decays. Solid lines should be compared to the data.

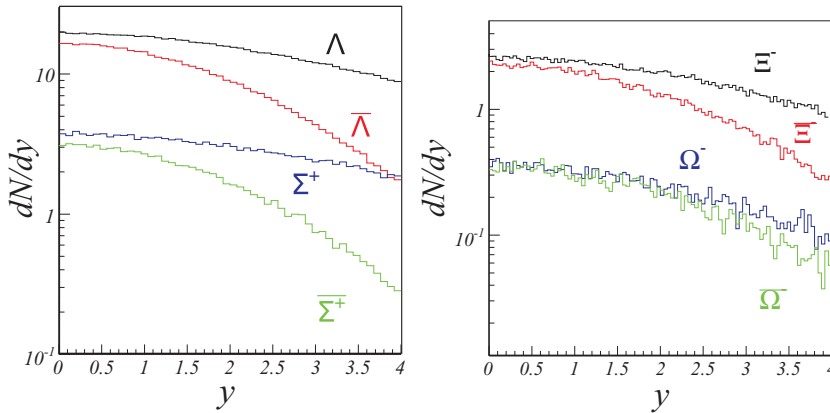


FIG. 9. (Color online) The model predictions for the rapidity spectra of hyperons. (Top) Curves from top to bottom: Λ , $\bar{\Lambda}$, Σ^+ , and $\bar{\Sigma}^+$. (Bottom) Curves from top to bottom: Ξ^- , $\bar{\Xi}^-$, Ω^- , and $\bar{\Omega}^-$. The model parameters as in Fig. 3.

source function. Thus at RHIC the proton and antiproton spectra may be qualitatively, but not quantitatively, explained on the ground of our statistical approach. It is not clear what the origin of the discrepancy is. We recall that also at midrapidity the single-freeze-out model has not reproduced the p and \bar{p} p_T spectra very accurately [59], only within 30–50% at low p_T (note, however, that the differences in the measurements for protons and antiprotons by various RHIC Collaborations are at the same level, as compared in the compilation of Ref. [60]). Rescattering of p and \bar{p} , found important in Ref. [54] and absent in our approach, is an obvious suspect. However, at the same time the single-freeze-out model reproduces very accurately the hyperon p_T spectra [36], indicating no need for rescattering in this case. More investigations to clarify the issue can be carried out with the help of abundant rapidity-dependence data for various particles from the NA49 Collaboration at SPS.

Figure 7 shows the p_T spectra at subsequent rapidity bins of the BRAHMS experiment. From top to bottom we have for pions $y \in [-0.1, 0.0]$, $[0.0, 0.1]$, $[0.4, 0.6]$, $[0.6, 0.8]$, $[0.8, 1.0]$, $[1.0, 1.2]$, $[1.2, 1.4]$, $[2.1, 2.3]$, $[2.4, 2.6]$, $[3.0, 3.1]$, $[3.1, 3.2]$, $[3.2, 3.3]$, $[3.3, 3.4]$, $[3.4, 3.66]$, and for kaons $y \in [-0.1, 0.0]$, $[0.0, 0.1]$, $[0.4, 0.6]$, $[0.6, 0.8]$, $[0.8, 1.0]$, $[1.0, 1.2]$, $[2.0, 2.2]$, $[2.3, 2.5]$, $[2.9, 3.0]$, $[3.0, 3.1]$, $[3.1, 3.2]$, and $[3.2, 3.4]$. Each lower curve is subsequently divided by the factor of 2 to avoid overlapping. The solid lines show the model calculation with optimum parameters (17). We note that the basic features of the experiment are reproduced, with the slope increasing with y . This can be explained with a lower transverse flow at larger y , as enforced by the parametrization (5). The quality of the agreement is similar in all rapidity bins. In Fig. 8 we give the similar study for the protons and antiprotons. The data points come from the BRAHMS Collaboration [34] and contain no weak-decay corrections, hence the solid lines should be compared to the data. Nevertheless, as in Fig. 6, we also present the calculation with feed-down from the weak decays switched off, as it provides a measure of systematic uncertainties. It should also be kept in mind that these uncertainties are quite large for the p_T spectra of p and \bar{p} , as can be inferred from the comparison of results of various experimental Collaborations at RHIC (cf. for instance Fig. 12 of Ref. [60]).

At this point we have accomplished the goal of fixing the “fireball topography”: we have the geometry/flow as well as thermal parameters dependent on the variable α_{\parallel} . Next, we

may proceed as in the case of the boost-invariant model used at midrapidity, and compute many observables in addition to those already used up to fix the model parameters. These observables include one-body observables, such as spectra of various particles, including hyperons, mesonic resonances, etc., as well as two-body observables related to correlations: HBT radii, balance functions in rapidity, or event-by-event fluctuations. Here we only present a sample prediction for rapidity spectra of hyperons, shown in Fig. 9. An interesting feature is the very small splitting of Ω and $\bar{\Omega}$, which results from the fact that $\mu_B - 3\mu_S \simeq 0$, cf. Fig. 2.

IV. CONCLUSION

The article contains results of the single-freeze-out-thermal model for rapidity-dependent spectra in relativistic heavy-ion collisions. We have used THERMINATOR to run the simulations and the BRAHMS data for $\sqrt{s_{NN}} = 200$ GeV Au+Au collisions to fix the model parameters. Such a simulation is necessary when the system is not boost invariant. It allows for an exact incorporation of the space-time dependence of thermal parameters, precise inclusion of resonance decays, as well as incorporation of experimental cuts. The extension of the original boost-invariant single-freeze-out model includes a modification of the shape of the fireball, which here becomes narrower as the magnitude of the spatial rapidity α_{\parallel} increases, as well as admits the dependence of the thermal parameters on α_{\parallel} . As a result of a fit to the BRAHMS data we have obtained the dependence of the freeze-out chemical potentials on α_{\parallel} . The freeze-out temperature is taken constant in the considered range of rapidities. With this extension we are able to properly describe the double $d^2N/(2\pi p_T dp_T dy)$ spectra from the experiment. We also make predictions for other particles, in particular for hyperons.

A code incorporating the elastic collisions neglected in the single-freeze-out approach could be used as an “afterburner” starting from our freeze-out condition. That way a more accurate collision picture could be achieved. As we have already mentioned, a recent study of Ref. [54] revealed that for the midrapidity p_T spectra the elastic rescattering is not very important.

Certainly, the scheme of this article can be used for other collisions where departures from the boost invariance are

significant, in particular for the rich SPS data. As we have said, the modeling involves the choice of the parametrization for the shape of the fireball and the velocity field of flow, where in fact we have quite a lot of freedom, as well as the dependence of the thermal parameters at freeze-out on the space-time position. Accurate data for numerous observables as functions of the rapidity, not only abundances and spectra but also the correlation data (HBT radii, balance functions), would greatly help to constrain the freedom and acquire insight into the space-time evolution picture of boost-noninvariant systems formed in relativistic heavy-ion collisions. Most importantly, the knowledge of the dependence of R_{side} on y would put constraints on the shape of the fireball.

Here are the main results of the article:

- (i) Naive extraction of the baryon and strange chemical potentials from ratios of p/\bar{p} and K^+/K^- works surprisingly well, as shown in the comparison to the full calculation in Fig. 2.
- (ii) The baryon and strange chemical potentials grow with α_{\perp} , reaching at $y \sim 3$ values close to those of the highest SPS energies of $\sqrt{s_{NN}} = 17$ GeV. This agrees with the recent conclusions of Roehrich [33].
- (iii) At midrapidity the values of the chemical potentials are even lower than derived from the previous thermal fits to the data for $|y| \leq 1$, with our values taking $\mu_B(0) = 19$ MeV and $\mu_S(0) = 5$ MeV. The reason for this effect is that the particle with $|y| \leq 1$ originate from a region $|\alpha_{\parallel}| \leq 2$, and on the average the effective values of chemical potentials are larger compared to the values at the very origin (cf. Fig. 2).
- (iv) The local strangeness density of the fireball is compatible with zero at all values of α_{\parallel} . Although this feature is natural in particle production mechanisms, here it

has been obtained independently just from fitting the chemical potentials to data.

- (v) The ratio of the baryon to strange chemical potentials varies very weakly with rapidity, ranging from ~ 4 at midrapidity to ~ 3.5 at larger rapidities.
- (vi) The $d^2N/(2\pi p_{\perp} dp_{\perp} dy)$ spectra of pions and kaons are well reproduced, supporting our hypothesis for the shape of the fireball in the longitudinal direction.
- (vii) The rapidity shape of the spectra of protons and antiprotons measured by BRAHMS [34] is described properly, while the model predicts a too large normalization, overproducing these particles by about 50%. This suggests a lower value of T by a few percent, or presence of nonequilibrium factors, not considered in this study. The effects of particle rescattering should also be considered, as inferred from Ref. [54]. We also note that the feature of an increasing yield of the net protons with rapidity is obtained naturally, explaining qualitatively but not quantitatively the shape of the rapidity dependence on purely statistical grounds.

More studies along the lines shown in this article, in particular at the lower SPS energies where abundant data are available for the rapidity and p_t spectra of various particles, will help to place bounds on the accuracy of the single-freeze-out approximation.

ACKNOWLEDGMENTS

We thank Wojciech Florkowski for his interest and numerous helpful comments. This research has been partly supported by the Polish Ministry of Education and Science, grant 2 P03B 02828.

-
- [1] BRAHMS Collaboration, Nucl. Phys. **A757**, 1 (2005).
 - [2] PHOBOS Collaboration, Nucl. Phys. **A757**, 28 (2005).
 - [3] STAR Collaboration, Nucl. Phys. **A757**, 102 (2005).
 - [4] PHENIX Collaboration, Nucl. Phys. **A757**, 184 (2005).
 - [5] P. Koch and J. Rafelski, South Afr. J. Phys. **9**, 8 (1986).
 - [6] J. Cleymans and H. Satz, Z. Phys. C **57**, 135 (1993).
 - [7] J. Sollfrank, M. Gazdzicki, U. W. Heinz, and J. Rafelski, Z. Phys. C **61**, 659 (1994).
 - [8] P. Braun-Munzinger, J. Stachel, J. P. Wessels, and N. Xu, Phys. Lett. **B344**, 43 (1995).
 - [9] P. Braun-Munzinger, J. Stachel, J. P. Wessels, and N. Xu, Phys. Lett. **B365**, 1 (1996).
 - [10] M. Gazdzicki and M. I. Gorenstein, Acta Phys. Polon. B **30**, 2705 (1999).
 - [11] G. D. Yen and M. I. Gorenstein, Phys. Rev. C **59**, 2788 (1999), nucl-th/9808012.
 - [12] J. Cleymans and K. Redlich, Phys. Rev. Lett. **81**, 5284 (1998).
 - [13] F. Becattini, J. Cleymans, A. Keranen, E. Suhonen, and K. Redlich, Phys. Rev. C **64**, 024901 (2001).
 - [14] J. Rafelski and J. Letessier, Phys. Rev. Lett. **85**, 4695 (2000).
 - [15] P. Braun-Munzinger, D. Magestro, K. Redlich, and J. Stachel, Phys. Lett. **B518**, 41 (2001).
 - [16] M. Michalec (2001), nucl-th/0112044.
 - [17] D. Magestro, J. Phys. G **28**, 1745 (2002).
 - [18] F. Becattini, M. Gazdzicki, A. Keranen, J. Manninen, and R. Stock, Phys. Rev. C **69**, 024905 (2004).
 - [19] P. Braun-Munzinger, K. Redlich, and J. Stachel, in *Quark Gluon Plasma 3*, edited by R. C. Itwa and X. N. Wang (World Scientific, Singapore, 2004).
 - [20] G. Torrieri and J. Rafelski, J. Phys. G **30**, S557 (2004).
 - [21] J. Cleymans, B. Kampfer, M. Kaneta, S. Wheaton, and N. Xu, Phys. Rev. C **71**, 054901 (2005).
 - [22] J. Rafelski, J. Letessier, and G. Torrieri, Phys. Rev. C **72**, 024905 (2005).
 - [23] F. Becattini and L. Ferroni, J. Phys. G **31**, S1091 (2005).
 - [24] G. E. Brown, J. Stachel, and G. M. Welke, Phys. Lett. **B253**, 19 (1991).
 - [25] J. Sollfrank, P. Koch, and U. W. Heinz, Phys. Lett. **B252**, 256 (1990).
 - [26] J. Bolz, U. Ornik, M. Plumer, B. R. Schlei, and R. M. Weiner, Phys. Rev. D **47**, 3860 (1993).
 - [27] W. Broniowski and W. Florkowski, Phys. Rev. Lett. **87**, 272302 (2001).
 - [28] W. Broniowski, A. Baran, and W. Florkowski, Acta Phys. Polon. B **33**, 4235 (2002).
 - [29] F. Cooper and G. Frye, Phys. Rev. D **10**, 186 (1974).
 - [30] S. A. Bass *et al.*, Phys. Rev. Lett. **81**, 4092 (1998).

- [31] J. Sollfrank, U. W. Heinz, H. Sorge, and N. Xu, Phys. Rev. C **59**, 1637 (1999).
- [32] A. Kisiel, T. Taluc, W. Broniowski, and W. Florkowski, Comput. Phys. Commun. **174**, 669 (2006).
- [33] D. Roehrich, talk at *Critical Point and Onset of Deconfinement* (Florence, 3–6 July, 2006).
- [34] I. G. Bearden *et al.* (BRAHMS), Phys. Rev. Lett. **90**, 102301 (2003).
- [35] I. G. Bearden *et al.* (BRAHMS), Phys. Rev. Lett. **94**, 162301 (2005), nucl-ex/0403050.
- [36] W. Broniowski and W. Florkowski, Phys. Rev. C **65**, 064905 (2002).
- [37] J. Rafelski, Phys. Lett. **B262**, 333 (1991).
- [38] T. Csorgo and B. Lorstad, Phys. Rev. C **54**, 1390 (1996).
- [39] K. Hagiwara *et al.* (Particle Data Group), Phys. Rev. D **66**, 010001 (2002).
- [40] C. M. Hung and E. V. Shuryak, Phys. Rev. C **57**, 1891 (1998).
- [41] E. V. Shuryak, Nucl. Phys. **A661**, 119 (1999).
- [42] S. A. Bass, A. Dumitru, M. Bleicher, L. Bravina, E. Zabrodin, H. Stoecker and W. Greiner, Phys. Rev. C **60**, 021902(R) (1999).
- [43] S. A. Bass and A. Dumitru, Phys. Rev. C **61**, 064909 (2000).
- [44] D. Teaney, J. Lauret, and E. V. Shuryak, Phys. Rev. Lett. **86**, 4783 (2001).
- [45] U. Heinz, Nucl. Phys. **A661**, 140c (1999).
- [46] W. Broniowski, W. Florkowski, and B. Hiller, Phys. Rev. C **68**, 034911 (2003).
- [47] P. Bozek, W. Broniowski, and W. Florkowski, Acta Phys. Hung. A **22**, 149 (2005).
- [48] W. Broniowski, A. Baran, and W. Florkowski, AIP Conf. Proc. **660**, 185 (2003), nucl-th/0212053.
- [49] A. Kisiel, W. Florkowski, W. Broniowski, and J. Pluta, Phys. Rev. C **73**, 064902 (2006).
- [50] D. Prorok, Eur. Phys. J. A **26**, 277 (2005).
- [51] D. Prorok, Eur. Phys. J. A **29**, 127 (2006).
- [52] D. Prorok, Phys. Rev. C **73**, 064901 (2006).
- [53] H. Sorge, H. Stoecker, and W. Greiner, Nucl. Phys. **A498**, 567c (1989).
- [54] C. Nonaka and S. A. Bass, Phys. Rev. C **75**, 014902 (2007).
- [55] W. Florkowski and W. Broniowski, Acta Phys. Polon. B **35**, 2895 (2004).
- [56] J. D. Bjorken, Phys. Rev. D **27**, 140 (1983).
- [57] J. Cleymans, H. Oeschler, K. Redlich, and S. Wheaton, J. Phys. G **32**, S165 (2006).
- [58] G. Torrieri *et al.*, Comput. Phys. Commun. **167**, 229 (2005).
- [59] A. Baran, W. Broniowski, and W. Florkowski, Acta Phys. Polon. B **35**, 779 (2004).
- [60] T. S. Ullrich, Nucl. Phys. **A715**, 399 (2003).